Penerbit Akademia Baru

Journal of Advanced Research in Fluid Mechanics and Thermal Sciences

Journal homepage: www.akademiabaru.com/arfmts.html
ISSN: 2289-7879

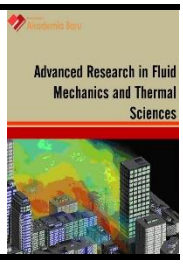


# Experimental and Numerical Study of Multiple Free Jet Impingement Arrays with $Al_2O_3$-Water Nanofluid

Open Access

Amr Mostafa Darwish[1,*], Abdel-Fattah Mohamed El-Kersh[2], Ibrahim Mahmoud El-Moghazy[2], Mohamed Naguib Elsheikh[3]

[1] Department of Mechanical Power Engineering, Faculty of Engineering, Beni-Suef University, Egypt
[2] Department of Mechanical Power Engineering, Faculty of Engineering, Minia University, Egypt
[3] Department of Mechanical Power Engineering, Faculty of Industrial Educational, Beni-Suef University, Egypt

**ARTICLE INFO**

***Article history:***
Received 9 September 2019
Received in revised form 23 October 2019
Accepted 11 November 2019
Available online 4 February 2020

**ABSTRACT**

Nanofluid jet impingement cooling is commonly used in many industrial applications due to its capability to dissipate large amounts of heat fluxes from surfaces. In this paper, an experimental and numerical investigation on heat transfer enhancement and fluid flow characteristics of multiple free surface jet impingement using water and $Al_2O_3$-water nanofluid as coolants were described. The effects of changing holes arrangement, nanofluid concentration and target to plate distance were investigated. Two jet arrays were employed; inline and staggered. A 3-D numerical calculations using Ansys CFX with standard k-ε turbulence model were presented. Results are obtained in terms of average Nusselt numbers, also the velocity, pressure, volume fraction and surface temperature contours were presented. The results show that, the best heat transfer enhancement was obtained at $H/D_{jet}$=20 using staggered jet arrangement. From experimental results, about 48% and 57% increase in average Nusselt number were obtained for inline and staggered jet arrays respectively at 6 m/s velocity and 10% nanofluid volume fraction. The numerical results presented good agreement with experimental results at low Reynolds numbers. Correlation equations were created to calculate Nusselt number for both inline and staggered jets cooling systems.

***Keywords:***
Nanofluid; jet impingement cooling; free surface flow; heat transfer enhancement

**Copyright © 2020 PENERBIT AKADEMIA BARU - All rights reserved**

## 1. Introduction

Jet impingement cooling technique is widely spread in many applications; heat treatment, drying, cooling of electronic chipsets, gas turbine blade cooling, food processing, plastic and glass tempering and processing of metals. Liquid jets may be classified as; free surface, confined, plunging, wall and submerged jets. Free surface jet is formed when the liquid is discharged in a gas medium. In the free surface jet configuration, the liquid release from nozzle plenum in a gas ambient which is mostly air before the impingement upon target plate [1]. The free surface appears immediately at the nozzle exit and continues to emerge all over the flow regime even at the wall-jet regions. The free surface

* *Corresponding author.*
*E-mail address: amr011309@eng.bsu.edu.eg (Amr Mostafa Darwis)*

jet shape can be specified by some factors; gravity, surface tension force and pressure force, while the position of gas/liquid interface can be determined by fulfilling the kinetic conditions and the harmony among shear and normal forces at this region [2]. About 30-50% augmentation in convection heat transfer coefficients was reached by combine the effects of turbulence on jet impingement cooling compared with laminar theory [3]. The free surface jets also can be classified as single or two phases jet depending on the working fluid employed in the cooling system. In the single-phase jet, air is used as a coolant which is discharged to ambient air and this process is called air entrainment. The second type is two-phase flow in which liquid jet is discharged in an air medium before it hitting the heated surface leading to increase in heat transfer performance due to the enhanced cooling capability of liquids compared to air which is employed in the single-phase flows [4].

Another category is single jet and multiple jet systems. In multiple jet impingement arrays, the interaction between jets affects heat transfer coefficients and its characteristics [5]. Hollworth and Berry [6] investigated heat transfer and fluid flow for an array of large jet-to-jet spacing square arrays with turbulent circular jet and minimum crossflow were employed, results show that, heat transfer coefficients were affected by the interference from neighbouring jets only for small jet-to-target spacing ($H/D_{jet} \leq 5$), for large jet-to-jet spacing ($X_n/D_{jet} \geq 20$) heat transfer coefficients didn't affected by varying the jet-to-target spacing. Obot and Trabold [7] investigated the effect of crossflow from spent air with different crossflow configurations; minimum, intermediate and maximum crossflow. A comparison between free and submerged arrays of jets were conducted experimentally by Robinson and Schnitzler [8], their results show that, for small $H/D_{jet}$ submerged jet arrays provide heat transfer enhancement more than free jet for the same Reynolds numbers. Geers *et al.,* [9] concluded that, Nusselt numbers decreased due to the wall jet velocity decreasing in the points between jets. Womac *et al.,* [10] correlated an equation for confined submerged and free jet impingement cooling, results show that, decreasing jet-to-jet spacing, increase heat transfer rate for free jet impingement. Brakmann *et al.,* [11] employed a 9×9 array of jet impinging on a flat plate to study heat transfer and pressure drop for a cooling system of turbomachinery, target was a plate with micro pin fins, they concluded that, maximum pressure drop found to be 14% in the comparison between smooth and finned targets, convective heat transfer increase by 135% to 142% when using finned target, however, the average Nusselt number ratio (Nu with fins/Nu without fins) decreased, maximum crossflow had a bad effect on the flow characteristics which deflect the jet and delay the impingement. Wan [12] conducted a comparison of multi jets impinging on a flat plate and roughened plate, inline one row of jets was employed, they concluded that, the highest average Nusselt number increased up to 162% with no pressure penalty compared with a flat plate. A large number of studies of multiple jet impingement using inline and staggered arrays were reviewed by Weigand and spring [13].

The traditional coolant such as water, oil and ethylene glycol show ineffectual behavior of heat transfer in many valuable industrial applications due to its low thermal conductivity and heat capacity [14]. Several experimental investigations were conducted to improve the thermo-physical properties of the coolants using the development in nanotechnology to create a solid particles in nanometer scale (smaller than 100 nm), then nanoparticles can dispersing in the base fluids according to Maxwell's equation to develop a new category of the two phase flow coolants termed as nanofluid. Nanofluid can enhance heat transfer process due to; 1- enhancing thermo-physical properties of the base fluid, 2- increase the surface area and heat capacity, 3- Intensifying the interaction collision between particles and hence reducing particles clogging compared with the conventional slurries. Wang Xiangqi [15] used different nanoparticles ($Al_2O_3$, CuO and CNT) and different volume fraction for laminar flow confined jet impinging. They found a 30% increase in Nusselt number in case of

alumina-water nanofluid at 10% volume fraction while 80% augmentation in Nusselt number was obtained in case of using CNT-water nanofluid at the same concentration. Palm *et al.,* [16] investigated $Al_2O_3$-water nanofluid with 38 nm in laminar flow jet impingement ($Re_{jet}$=500:946), the best volume fraction was 7.5% to achieve 70% Nusselt number. Yang and Lai [17] used alumina-water nanofluid with 7.5% concentration by volume and 47 nm nanoparticles diameter and they observed 70% augmentation in average Nusselt numbers. Freng [18] used $Al_2O_3$ water with 30 and 47 nm size and laminar flow jet impingement ($Re_{jet}$ <800). It was found that the best concentration was 4%, nanofluids are a smoother mixture flow fields when compared with water as a base fluid.

Heat transfer enhancement using nanofluid jet impingement was affected by; nanofluid concentration (volume fraction), nanoparticles type and size, and turbulence. Kumar and Mulugeta [19] investigated nanofluid jet impingement using array of jets. They investigated experimentally inline array of jets impinging on a finned plate heat sink using $Al_2O_3$-water nanofluid. Ultrasonic bath was used to disperse the nanoparticles into the base fluid for 6 hrs. Two-step method was used to prepare the nanofluid with ϕ=0.1% concentration. They concluded that, adding nanoparticles to water increase the heat transfer coefficients by 32.92% at 0.1% concentration of $Al_2O_3$ in water. Manca *et al.,* [20] studied numerically heat transfer enhancement of a two-dimensional nanofluid slot jet impingement using $Al_2O_3$- water with 38 nm particle size and different concentrations. They concluded that, increasing nanofluid concentration causes an increase in the bulk temperature because of increasing thermal conductivity of the mixture. Average Nusselt number increased by 18% at 6% nanofluid concentration and the pumping power was increased by increasing nanofluid concentration and jet velocity. Armaghani *et al.,* [21] studied numerically two-dimensional flow and heat transfer characteristics of plane jet by using DNS (direct numerical simulation) model, $Al_2O_3$-water and CuO-water were employed as a heat transfer carrier and the concentration varied from 0 to 4%. They found that $Al_2O_3$-water nanofluid enhances heat transfer greater than CuO for the same volume fraction and the turbulent intensities in $Al_2O_3$ was found to be higher than that in CuO. Another two-dimensional simulation using two-phase mixture model was conducted by Huang and Jang [22]. They concluded that, SST k-ω turbulence model is an appropriate to determine the average Nusselt and 16% of heat transfer enhancement was obtained with 5% concentration and $H/D_{jet}$=5. Siddiqui and Jha [23] concluded that, in case of free surface flow domain with gas-liquid interface, the results of k-e turbulence models have a good agreement with the experimental results compared with other models. Yang *et al.,* [24] applied Siddiqui and Jha [23] technique in the jet impingement cooling application. Another investigation of multiphase flow simulated by Davarnejad and Jamshidzadeh [25], they reported that, k-ε turbulence model results are exhibiting a good performance than k-ω turbulence model when compared with experimental results. Isman *et al.,* [26] reported that standard k-ε turbulence model obtained more reliable results with 10% max variation when compared with measured values than RNG k-ε turbulence model for the jet impingement application. Roy *et al.,* [27] employed alumina-water nanofluid with different concentration and found 110% of Nusselt number augmentation at 10% nanofluid volume fraction. Hasan *et al.,* [28] applied nanofluid multiple jet impingement cooling technique on photovoltaic thermal (PVT) collector, different types of nanoparticles (SiC, $TiO_2$ and $SiO_2$) were dispersed into water with 1% volume concentration, they concluded that, using Sic-water nanofluid jet impingement cooling can enhance thermal and electrical performance of the PVT system by 97.95 % compared with traditional system.

As reviewed above, the most previous studies of free surface jet impingement were conducted using air or water as a working fluid, while a few studies employed nanofluids as coolants in a single nanofluid free surface jet impingement cooling system and no studies were conducted using multiple nanofluid free surface jets impinging on a heated flat plate. Numerical analysis of free surface jet

impingement includes a complex tracking of the free surface in the turbulent regime between air entrainment and the fluid jet is considered to be a challenge using a single jet while, the big challenge when a jet array is employed where, jet to jet interfaces has an effect on heat transfer and fluid flow characteristics, hence, the present study is focused on using different arrays of free surface jets and investigate (experimentally and numerically) its effects on nanofluid jet impingement cooling system.

## 2. Experimental Analysis

### *2.1 Apparatus*

An experimental test rig is constructed to study heat transfer performance and fluid flow features of $Al_2O_3$-water nanofluid in a free surface multiple jet impingement cooling system (as shown in Figure 1). Liquid (water or nanofluid) is pumped from the main tank (19) by using 1 HP centrifugal pump (1) through 0.5-inch stainless steel pipes to the plenum chamber (7) and jets plate (8) before hitting the target plate (9). The falling liquid after impingement is collected in the collecting tank (15), and then it passes through a coil heat exchanger (17) to maintain jet temperature at 298 K, finally the liquid return to the main tank to be recycled again in the system. A calibrated turbine flow meter (4) with accuracy of ±1% of reading (NUFLO MC-II flow analyzer from Cameron) is installed in the test rig to measure the flow rate, while the flow rate is controlled using a calibrated bypass control valve (3).

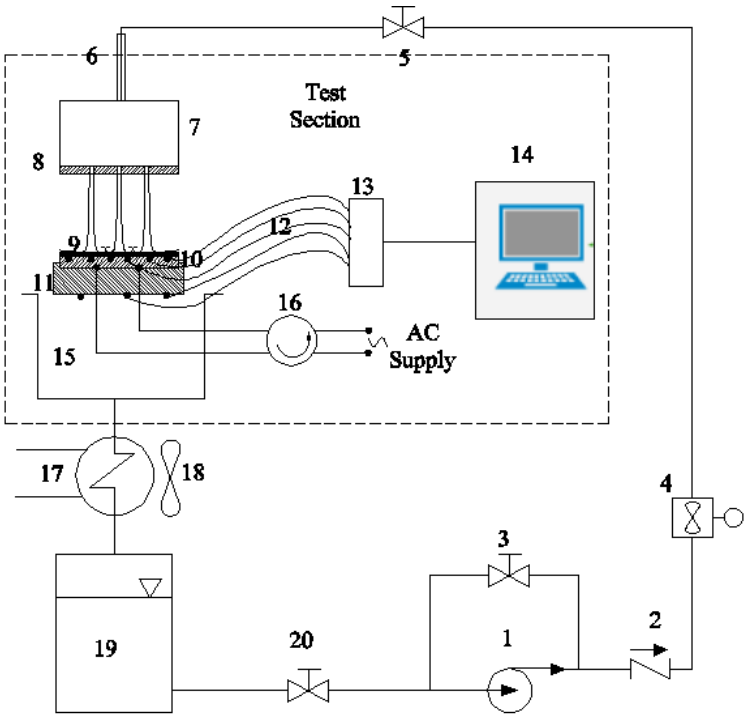


1- Pump
2- Check Valve
3- Control alve
4- Turbine flowmeter
5- Discharge valve
6- Traversing mechanism
7- Plenum
8- Jets plate
9- Target plate
10- Heater
11- Insulation
12- Thermocouples
13- Data acquisition
14- Computer
15- Collecting tank
16- VARIAC Transformer
17- Heat exchanger
18- Fan
19- Main tank
20- Suction valve

**Fig. 1.** Test rig schematic diagram

The test section is shown in Figure 2 and consists of plenum chamber (7) which is supplied from 0.5-inch pipe, the importance of the plenum chamber is to ensure equal flow rate in all jets, and flow passes from the supply pipe to fill the plenum chamber before out from the jets plate. A stainless steel target plate (9) (150x150x2 mm) is heated by a nickel chrome strip heater (10) is designed to generate constant heat flux, electrical power supplied to the heater is controlled by using VARIAC transformer (16) so that , heat flux can be controlled. Heater upper surface is in well contact with the target bottom surface while the lower surface of the heater is well isolated by using 100 mm glass wool (k= 0.04 W/m.k at 298 K) followed by 100 mm of wood (k=0.17 W/m.k at 298 K) (11). A set of calibrated type J thermocouples (12) are designed and installed on the target plate, on the back surface of the insulation to measure the heat losses, on the jets plate to measure the jet temperature ($T_{jet}$) , in the outlet of cooling system and in the main and collecting tanks, the milli-volt from thermocouples is measured by using two 1216 PICO log multi-channels data acquisition systems (16 channels) (13) with accuracy of ± 0.5% at 12 bits resolution of reading and then the data are monitored in the computer (14). Jet-to-target spacing can be controlled by the traversing mechanism (6).

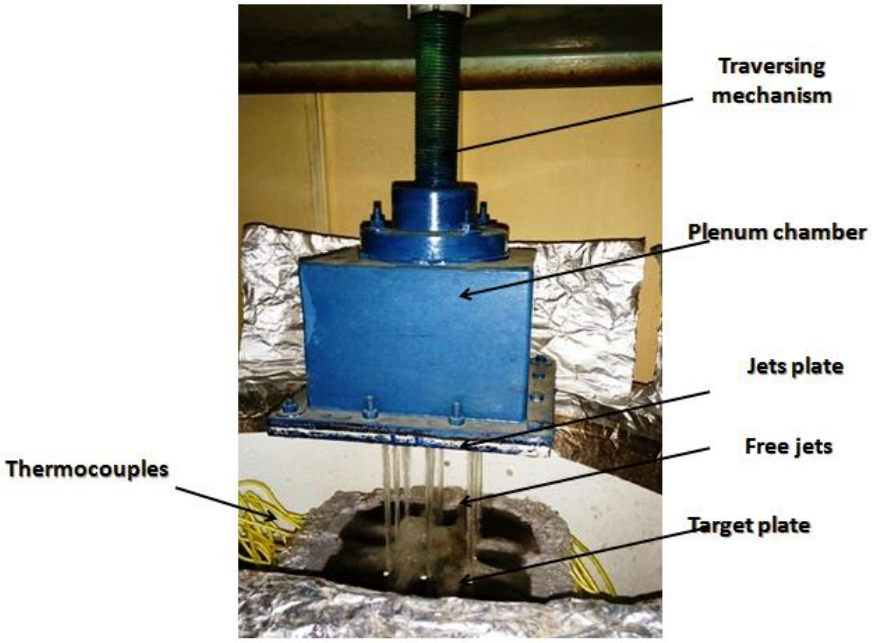


**Fig. 2.** Photography of the test section

Some of the geometrical parameters are selected according to the previous studies while the effects of changing some other parameters are investigated, $X_n/D_{jet}$=7, $H/D_{jet}$= 10, 20, 30 and 40, $Re_{jet}$=5600 to 33610 (for water), jet temperature=298 K, nanofluid concentration=5%, 8% and 10%, nozzle diameter =5 mm.

As mentioned above in the literature inline and staggered arrays were investigated using water or air as a working fluid hence, in this study, two jet configurations are considered using nanofluid; 9 inline jet array and 10 staggered jet array as shown in Figure 3.

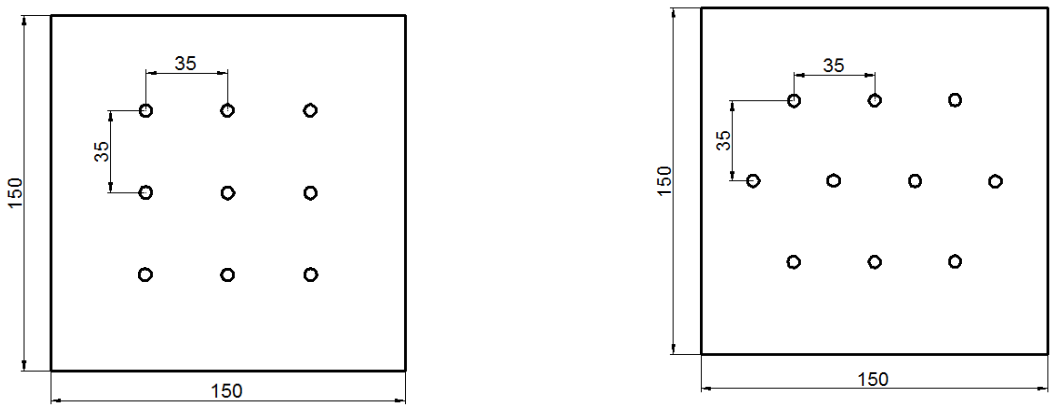


(a) (b)

**Fig. 3.** Configurations of jet arrays; a- inline array, b- staggered array

### *2.2 Experimental Procedures*

The following steps are conducted for each experiment.

i. At the beginning of each experiment, the target plate is cleaned with acetone
ii. Ensure that all fittings and parts are sealed with thermal silicone to prevent leakage.
iii. Ensure that, pump discharge line is full of water to prevent cavitation or any damage in the impeller.
iv. Set the jet-to-target spacing by using the traversing mechanism.
v. Turn on the DAQ system and check thermocouples connections to ensure that the connection doesn't lose and input into the proper channel.
vi. Turn on pump after ensuring that the bypass valve is open to the desired flow rate.
vii. Turn on the electrical heater and set the VARIAC to the required heat flux.
viii. Allow the system to run until all thermocouples reached to a uniform reading (about 30 minutes).
ix. Thermocouples readings were collected by DAQ system and recorded to the computer.
x. Repeat the previous stages with different flow rates and different jet configurations.
xi. Now the experiment is finished, turn the heater off and don't shut down the pump until the target temperature level is in the safe range.

### *2.3 Data Reduction*

The properties of water are taken at the film temperature

$$T_f = \frac{T_{avg}+T_{jet}}{T_{jet}} \ (K) \tag{1}$$

where $T_{avg}$ is the average surface temperature. The jet Reynolds number (based on nozzle diameter) calculated from

$$Re_{jet} = \frac{\rho.V_{jet}.D_{jet}}{\mu} \tag{2}$$

Average heat transfer coefficient can be calculated from

$$h_{avg} = \frac{q_{net}}{T_{avg} - T_{jet}} \left(\frac{J}{m^2.K}\right) \quad (3)$$

where $q_{net}$ is the net heat flux with neglecting the heat losses from the back surface of the heated plate W/m$^2$.

$T_{avg}$ is the average surface temperature on the target plate (K). Average and Nusselt number based characteristic length of the heated plate is calculated from

$$Nu_{avg} = \frac{h_{avg}.L}{k} \quad (4)$$

*2.4 Nanofluid Preparation and Properties*

*2.4.1 Nanofluid preparation*

In the present study, two-step preparation technique is used to prepare and disperse $Al_2O_3$ nano powder in water. Nanoparticles concentrations of 5%, 8% and 10% by volume are employed. To increase the nanofluid stability, the mixture is put in a magnetic stirring for 12 hrs at 3500 rpm and then put in a bath of ultrasonic vibration for 1.5 hrs which is the optimum time to make a good stability [29]. Sodium dodeobcyl benzene sulfonate (SDBS) surfactant with 1% concentration by weight is added to the mixture for better dispersing and preventing the nanoparticles participation while higher surfactant concentration is not recommended which reduce thermal conductivity of nanofluid [30]. The nanofluid preparation sequence and procedures is shown in Figure 4.

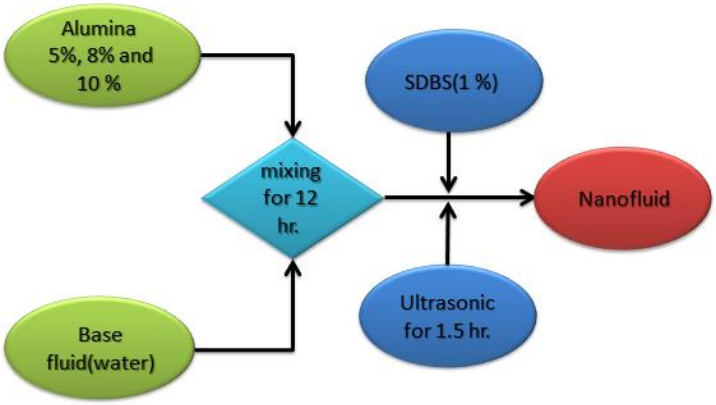


**Fig. 4.** Nanofluid preparation process procedures

*2.4.2 Nanofluid properties*

Many investigations focused on measuring and calculating the nanofluid properties. Maxwell [31] created a correlation for the effective thermal conductivity of liquid-solid mixture, but their equation is more suitable for milli or micro particles suspended in base fluid and they neglect the effects of particles motion into the base fluid. Bruggeman [32] attributed the enhancement of thermal conductivity due to particles interactions which include; particle-particle, wall- particle and liquid-particle interactions, he developed a thermal conductivity correlation which is suitable for nanofluids. Xuan *et al.,* [33] proposed a model considering the effects of nanoparticles motions in the base fluids which is called Brownian motion, on thermal conductivity enhancement of nanofluids, their correlation consists of two terms, one of Maxwell's model and the other term is due to Brownian

motion. Table 1 summarizes the properties of water at 298 K (from ASHRE handbook [34]) and $AL_2O_3$ nanoparticles. Table 2 illustrates the thermo-physical properties correlations of $Al_2O_3$-water nanofluid (Li *et al.,* [35]).

**Table 1**
Properties of water at 298 K and alumina nanoparticles

| Material | ρ(kg/m3) | μ(Pa.s) | Cp(J/kg.K) | k(W/m.K) | Dp(nm) |
|---|---|---|---|---|---|
| Water | 996 | 0.000889 | 4143 | 0.61 | - |
| $Al_2O_3$ | 3880 | - | 773 | 36 | 20 |

**Table 2**
Alumina-water nanofluid properties equations

| Thermo-physical property | Empirical formula |
|---|---|
| Density ($\rho_{nf}$, kg/m3) | $(1-\varphi)\rho_b + \varphi\rho_p (5)$ |
| Dynamic viscosity ($\mu_{nf}$,Pa.s) | $\mu_{nf} = \mu_b(123\varphi^2 + 7.3\varphi + 1)$ (6) |
| Thermal conductivity ($k_{nf}$, W/m.K) | $k_{nf} = 0.25\left[(3\varphi-1)k_p + (2-3\varphi)k_b + \sqrt{\Delta}\right]$ (7)<br>$\Delta = \left[(3\varphi-1)k_p + (2-3\varphi)k_b\right]^2 + 8k_pk_b$ (8) |
| Heat capacity ($Cp_{nf}$, J/kg.K) | $\frac{(1-\varphi)Cp_b\rho_b + \varphi Cp_p\rho_p}{\rho_{nf}}$ (9) |

*2.5 Uncertainty Analysis*

The basic quantity observed directly from the laboratory is called variable (v) and the data are a group of variables while the results (R) are obtained by correcting the data. It's important to obtain the effects of the uncertainty on the experimental results. If the result is function of n number of variables [36].

$$R = R(v_1 + v_2 + v_3 + \dots\dots\dots\dots v_n) \quad (10)$$

Then the relation of the uncertainty of these variables ($w_v$) and the uncertainty of the result ($w_R$) can be obtained in general as (Kline, S. J [36])

$$w_R = \sqrt{\left(\frac{\partial R}{\partial v_1}w_{v_1}\right)^2 + \left(\frac{\partial R}{\partial v_2}w_{v_2}\right)^2 + \cdots\left(\frac{\partial R}{\partial v_n}w_{v_n}\right)^2} \quad (11)$$

The relative error of temperature is estimated to be ± 0.5%, target and jets plate length and jet diameter are measured by digital Vernier within an accuracy of ± 0.1 mm, the relative error of target plate and jet area are calculated and maintained at ±1.3% and ±0.04% respectively. A PICO log multi-channel data acquisition system (16 channels) is used with a digital voltmeter of the accuracy of ± 0.5% of reading. Electric heater voltage and current are measured using fluke clamp meter with ± 1 V accuracy for voltage and ± 0.01 A for current. A calibrated turbine flow meter with an accuracy of ±1% of reading (NUFLO MC-II flow analyzer from Cameron) is installed in the test rig to measure the flow rate. Maximum uncertainty of Jet Reynolds numbers is estimated to be 4.3%. The maximum uncertainty of heat transfer coefficients for inline and staggered jets are 3.5% and 3.9% respectively. The uncertainty of Nusselt number is 5.2% and 5.6% for inline and staggered jets respectively.

## 3. Numerical Analysis

### *3.1 Problem Description*

Computational fluid dynamics provides us with a lot of details which is difficult to analyze experimentally, 3-D domains are employed for a good understanding of heat transfer behavior of multiple free surface jet impinging on a flat plate under the same experimental parameters ($H/D_{jet}$, $Re_{jet}$, $X_n/D_{jet}$, heat flux and volume fraction). A 3-D steady-state Navier-Stokes and energy equations for incompressible flow in the Cartesian coordinates are employed; a cooling jet is released from the nozzles plenum before hitting the stainless-steel target plate. Air entrainment is represented by a cubical extended domain to prevent the backflow Figure 5. Zhang and Faghri [37] found that, the heat transfer behavior and fluid flow characteristics of alumina –water nanofluid depends mainly on the fluid temperature, shear rates, nanoparticle diameter, shape and its volumetric concentration. Sahoo *et al.,* [38] experimentally found that Alumina-water nanofluid behaved like a Newtonian fluid at a higher temperature (0-90°C) with 1-10% volume concentrations prepared by 53 nm $Al_2O_3$ nanoparticles dispersed in a base fluid. Tang *et al.,* [39] found that, the viscosity and friction factor of alumina nanoparticles dispersed in water at 6% volume fraction flowing inside circular tube exhibits Newtonian behavior for operating temperature between 6 to 75°C, therefore, the alumina-water nanofluid at concentration below 10% can behave as a Newtonian fluid. The present investigation is more concentrated on the thermo-physical behaviour of the coolant and external properties of the impingement jet and the results are introduced in the form of velocity, pressure, temperature and liquid volume fraction contours of water and nanofluid. To create a mathematical formulation for the proposed numerical model, the following assumptions are considered.

i. The Newtonian fluid flow of nanofluid assumed to be steady, turbulent and incompressible with uniform inlet velocity
ii. For water and nanofluid the single phase model is adopted
iii. The physical properties of water and nanofluid assumed to be constant

No slip condition has been applied to hot and cold walls.

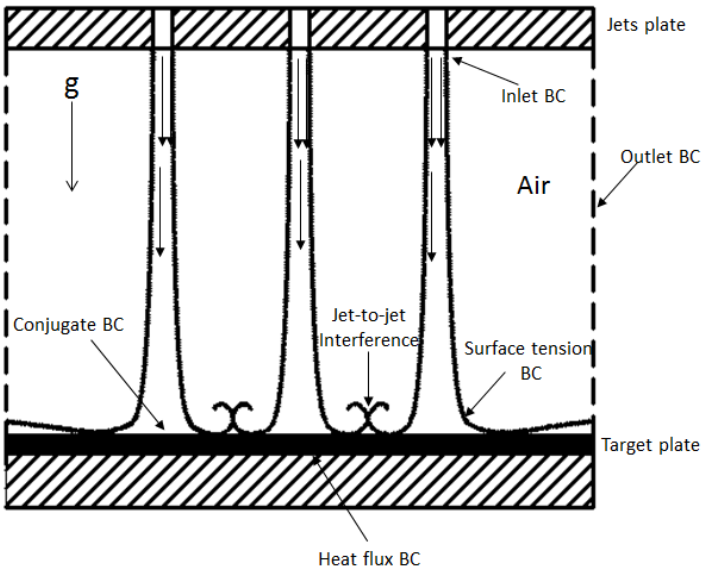


(a)

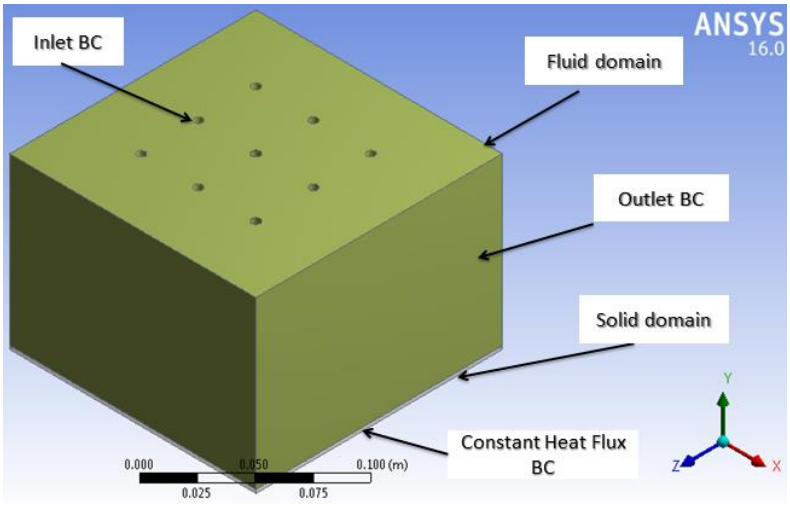


(b)

**Fig. 5.** (a) Domain description and (b) boundary conditions

### *3.2 Governing Equations*

Multiphase flow is employed in the present study in which, the static air surrounding the computational domain is considered to be the secondary phase while the fluid from the nozzles is the primary phase. Computational model includes the free surface between the fluid jet and air entrainment has been proposed, that requires an accurate tracking throughout the computational domain with the multiphase algorithm thus Ansys CFX free surface model is employed to collect the sharp interface between the two fluids inside the computational domain. A set of equations solved by Ansys CFX are the incompressible, unsteady Navier-stokes equations in their conservation form. In this section instantaneous equations of mass, momentum and energy conservation are presented in its basic and phasic forms [40]

Continuity equation

$$\frac{\partial(\rho_{nf})}{\partial t} + \nabla.\left(\rho_{nf}U\right) = 0 \tag{12}$$

where, U is the mean velocity, $\rho_{nf}$ is the nanofluid density and $\nabla$ is the vector operator

Momentum equation

$$\frac{\partial(\rho_{nf}U)}{\partial t} + \nabla.\left(\rho_{nf}.U * U\right) = -\nabla P + \nabla.\tau + S_M \tag{13}$$

where, P is the mean pressure, $S_M$ is the momentum source and $\boldsymbol{\tau}$ is the stress tensor = $\mu(\nabla U + (\nabla U)^T - \frac{2}{3}\delta\nabla U)$

Total energy equation

$$\frac{\partial(\rho_{nf}h_{tot})}{\partial t} - \frac{\partial P}{\partial t} + \nabla.\left(\rho_{nf}Uh_{tot}\right) = \nabla.(K\nabla T) + \nabla.(U.\tau) + U.S_M + S_E \tag{14}$$

where, $h_{tot}$ is the specific total enthalpy, k is the thermal conductivity and $S_E$ is the energy source.

### 3.3 Turbulence Modeling

Standard k-ε turbulence model is employed in the present simulation to formulate the incompressible turbulent flow and heat transfer problem with steady state condition, this semi-empirical model is based on transport equations for turbulence kinetic energy (k) and its dissipation rate (ε), the governing equations can be written as

Phasic transport equation for k [40]

$$\frac{\partial}{\partial t}(r_\alpha \rho_\alpha k_\alpha) + \nabla\left[r_\alpha\left[\rho_\alpha U_\alpha k_\alpha - \left[\mu + \frac{\mu_{t\alpha}}{\sigma_k}\right]\nabla k_\alpha\right]\right] = r_\alpha(P_\alpha - \rho_\alpha \varepsilon_\alpha) + T_{\alpha\beta}^{(k)} \quad (15)$$

Phasic transport equation for ε

$$\frac{\partial}{\partial t}(r_\alpha \rho_\alpha \varepsilon_\alpha) + \nabla\left[r_\alpha \rho_\alpha U_\alpha \varepsilon_\alpha - \left[\mu + \frac{\mu_{t\alpha}}{\sigma_\varepsilon}\right]\nabla \varepsilon_\alpha\right] = r_\alpha \frac{\varepsilon_\alpha}{k_\alpha}(C_{\varepsilon_1} P_\alpha - C_{\varepsilon_2}\rho_\alpha \varepsilon_\alpha) + T_{\alpha\beta}^{(\varepsilon)} \quad (16)$$

where $T_{\alpha\beta}^{(k)}$ $and$ $T_{\alpha\beta}^{(\varepsilon)}$ are the interphase transfer for k and ε respectively.

Phasic turbulent viscosity is modeled as

$$\mu_{t\alpha} = C_\mu \rho_\rho (\frac{k_\alpha^2}{\varepsilon_\alpha})$$

where $C_{\varepsilon_1}$=1.44, $C_{\varepsilon_2}$=1.92, $\sigma_k$=1, $\sigma_\varepsilon$=1.3, $C_\mu$=0.09, $P_\alpha = \tau_{ij}\frac{\partial U_i}{\partial X_j}$

### 3.4 Boundary Conditions

#### 3.4.1 Inlet boundary

A discrete model was created to simulate the entrance condition of the present study where the results of velocity components (u,v,w) at the nozzles exit are exported as inlet condition to the present model.

v= - Vjet, u=w= 0, $T_f$=$T_{jet}$, $k_{jet} = \frac{3}{2}(iV_{jet})^2$, $\varepsilon_{jet} = C_\mu^{\frac{3}{4}}(\frac{k_{jet}^{3/2}}{l})$

where i is the turbulence intensity and *l* is the turbulent length scale of the fluid domain inlet.

#### 3.4.2 Outlet boundary

The four sides of the fluid domain were set to an entrainment opening with zero static pressure in order to let the air flow in and out without any specific direction.

$P=P_{atm}$

$$\frac{\partial u}{\partial n} = \frac{\partial v}{\partial n} = \frac{\partial w}{\partial n} = \frac{\partial T_f}{\partial n} = \frac{\partial k}{\partial n} = \frac{\partial \varepsilon}{\partial n} = 0$$

### *3.4.3 Conjugate boundary*

The upper surface of the solid domain was set as conjugate heat transfer in which energy equation is solved but with no flow.

u=v=w=0, $T_f=T_s$ and $k_s \frac{\partial T_s}{\partial n} = k_f \frac{\partial T_f}{\partial n}$

i. Bottom wall heat flux boundary

$$q^{``} = -k_s \frac{\partial T_s}{\partial n} = Constant$$

ii. Other walls
All solid domain sides (except upper and bottom) estimated to be no slip condition walls

iii. Interfaces
The fluid-solid domains interface is automatically identified by Ansys CFX solver

### *3.5 Meshing and Grid Independence*

In the meshing stage, solid and fluid bodies are divided into sufficiently small discrete volumes. A fine mesh is required in calculating the variables gradients more than coarse mesh. Applying a refinement on some regions in the computational domain is the most important one, where large flow fluctuations are expected in these regions, however, applying fine mesh consumes more power and time, so, a grid independence study is required for meshing optimization, the mesh size is refined gradually (starting with coarse grid) until constant results are obtained so that, results are no longer affected by any more refinements, a special refinement is done about the centerline of the jet, in the fluid-solid interface region, in the jet entrance region and, about the stagnation zone on the solid domain , Figure 6 shows the 3-D computational grid arrangement of the inline jet array. Six fine grids with a different number of elements are examined in the grid independence test; grid1=1662054 cell, grid2=2358629 cell, grid3=2711977 cell, grid4=3384441 cell, grid5=5934513 cell and grid6=7336700 cell (very fine). The relation between a number of elements in each grid and the maximum temperature on the target plate, at $V_{jet}$=3 m/s, $X_n/D_{jet}$=7 and $H/D_{jet}$= 20 and 20 kW/m$^2$ heat flux is shown in Figure 7, it can be illustrated from the curve that, the solution is a grid-dependent at the grid 4 with very small deviation, hence, grid 4 with 3384441 elements is suitable enough to simulated heat transfer and fluid flow of inline jet impingement cooling. The same test is conducted on the staggered jet configuration and the optimum grid size is 3918560 cells.

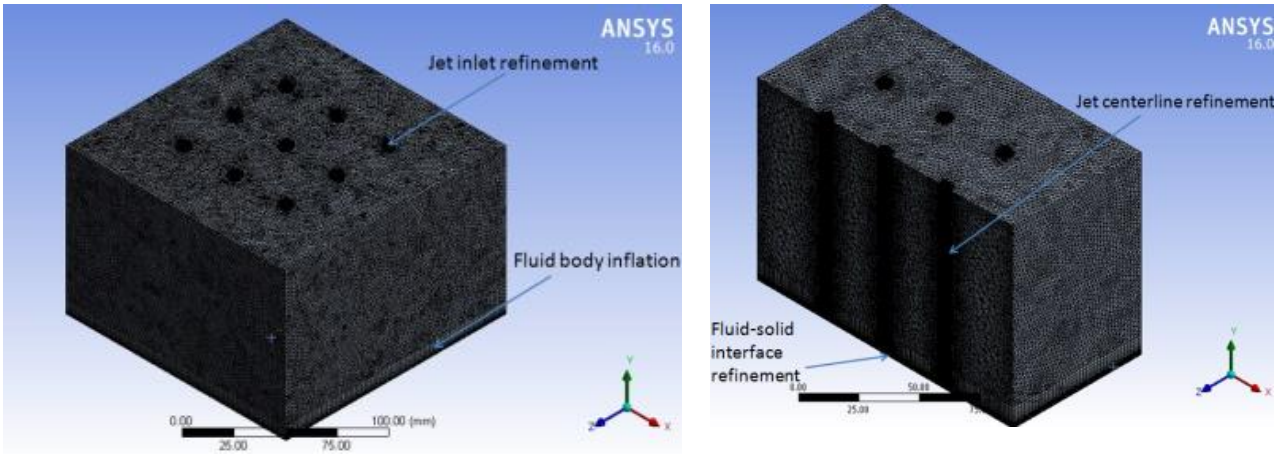


(a)

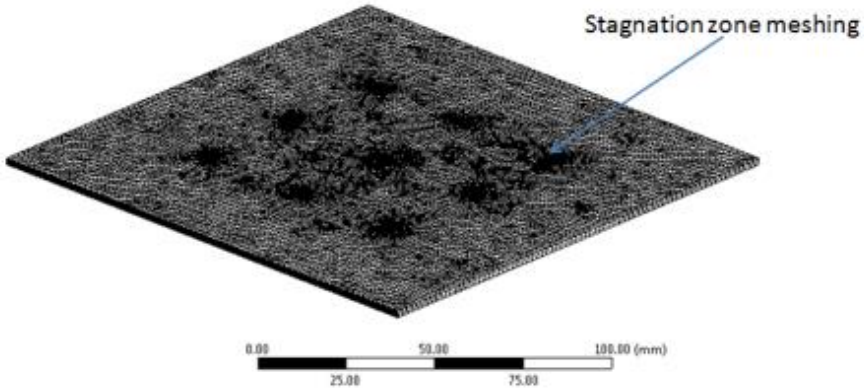


(b)

**Fig. 6.** 3-D computational mesh design of inline jet impingement array

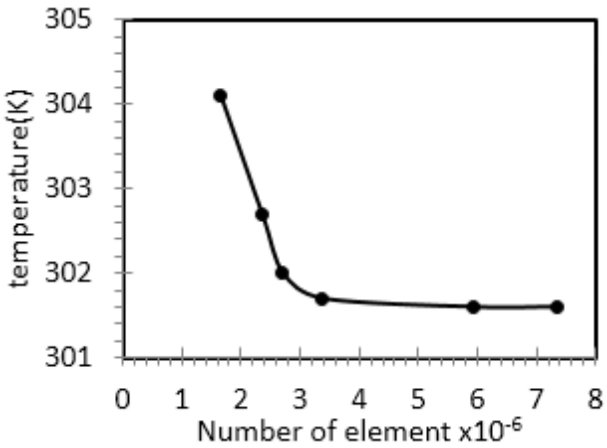


**Fig. 7.** Relation between grid size and maximum Temperature on the target plate

Flow models and initial flow conditions and other numerical setting in CFX code which are summarized in Table 3.

**Table 3**
General numerical settings

| Parameter | Setting |
|---|---|
| Model | Steady state |
| Turbulence | Standard k-ε |
| Advection scheme | High resolution |
| Turbulence numeric | High resolution |
| Timescale factor | 1 |
| Residuals type | RMS |
| Residuals target | $10^{-4}$ for all equations |
| Free surface model | standard |
| Multiphase model | homogeneous |
| Buoyancy model | Buoyant |
| Fluid buoyancy model | Boussinesq |
| Buoy ref. Temp. | 298 K |
| Inter-phase compression level | 2 |
| Inter-phase transfer | Free surface |
| Volume fraction | Coupled |

### *3.6 Code Validation*

The importance of the validation process is to check the agreement of the numerical results with the experimental results. Numerical and experimental results for inline and staggered jets are obtained in Figure 8 as a relation between average Nusselt numbers with jet Reynolds numbers at $H/D_{jet}=20$, $X_n/D_{jet}=7$ and $Re_{jet}$ varied from 2440 to 14640, the working fluid is Alumina-water nanofluid with 10% concentration at jet temperature of 298 K and a 30 kW/m$^2$ constant heat flux is applied to the target plate. Generally, the numerical results are in a good agreement with the experimental results in the low Reynolds range and the numerical values are overestimated for high Reynolds numbers. The maximum deviations in average Nusselt numbers were 14.3% and 9.1% for inline and staggered jet arrays respectively at $V_{jet}=6$ m/s and these results ensure that the present model is suitable for simulating heat transfer and fluid flow for both single or multiple free surface jet impingement cooling systems however, it is not recommended for the high jet Reynolds number applications (gas turbine blade cooling application).

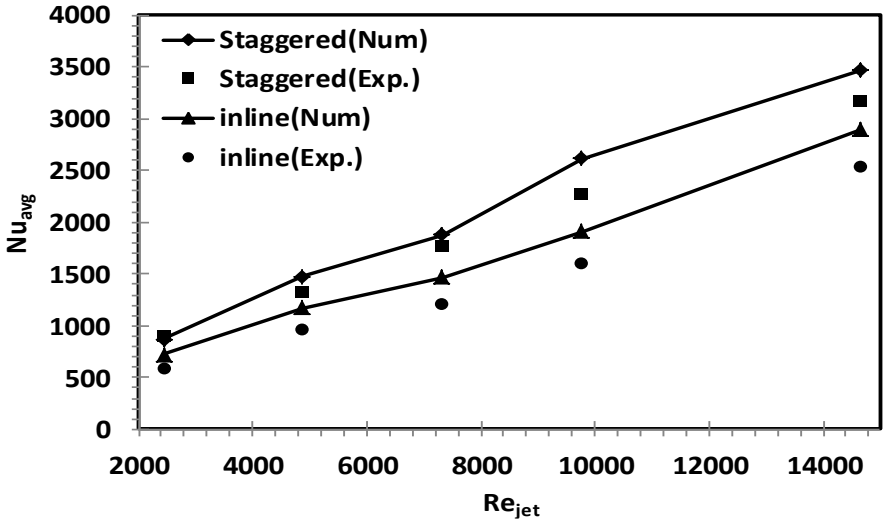


**Fig. 8.** Comparison between Experimental and numerical results for inline and staggered jet configurations at 10% alumina-water concentration

## 4. Results

### *4.1 Fluid Flow Structure*

Flow structure of the impinging jets plays an important role to understand the hydrodynamics of the jet impingement cooling system. Contours are obtained on a plane shown in Figure 9. Figure 10 shows the distributions of water volume fraction, water velocity, static pressure and target temperature, water at 298 K is employed as a coolant with $V_{jet}$=6 m/s. The flow structure of the impingement jet include four characteristic regions; potential core region, developing region, stagnation region and wall jet region, in the potential core the velocity is constant and equal to the velocity at the nozzle exit, In the developing flow part, there is a decay of the centerline velocity and this followed by a fully developed flow part where the velocity profiles are similar, in the wall jet region the boundary layer thickness increases while the flow is leaving the stagnation region (Figure 10(a)). At the stagnation region, the static pressure increased quickly due to the axial velocity degradation (Figure 10(b)). A sharp interface between water and air entrainment is presented in Figure 10(c), after jet hitting the target, the water film thickness increase due to the water jump phenomenon. The temperature distribution on the target plate is presented in Figure 10(d), the lowest temperature recorded at the stagnation zones and the highest temperature recorded at the target edges which are far away from the impingement zone. Water splashing effect is increased with increasing jet velocity, this effect can increase heat transfer rate and reduce average temperature on the hot plate.

Increasing jet velocity leads to increase the jet-to-jet interference and inflow recirculation between jets which explain the reduction of heat transfer rate between jets (as shown in Figure 11). Velocity contours, Surface temperature contours and Water volume fraction rending for inline and staggered arrays are presented in Figure 12- 14.

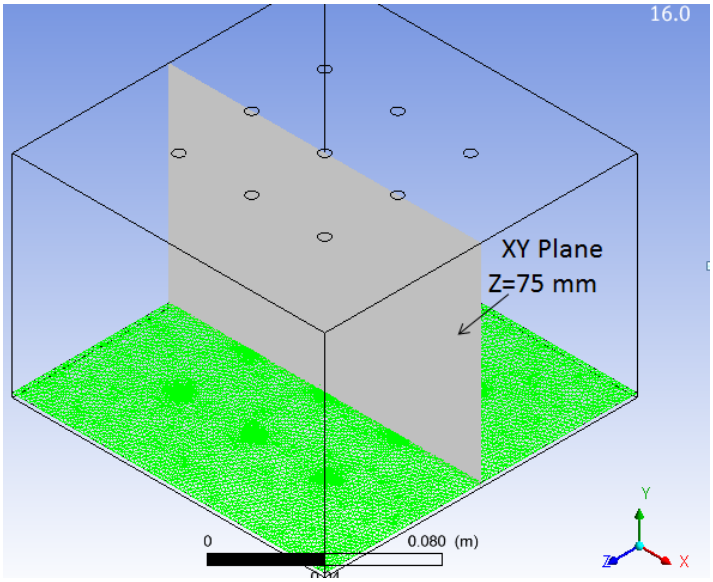


**Fig. 9.** Location of xy plane that the contours are illustrated on it

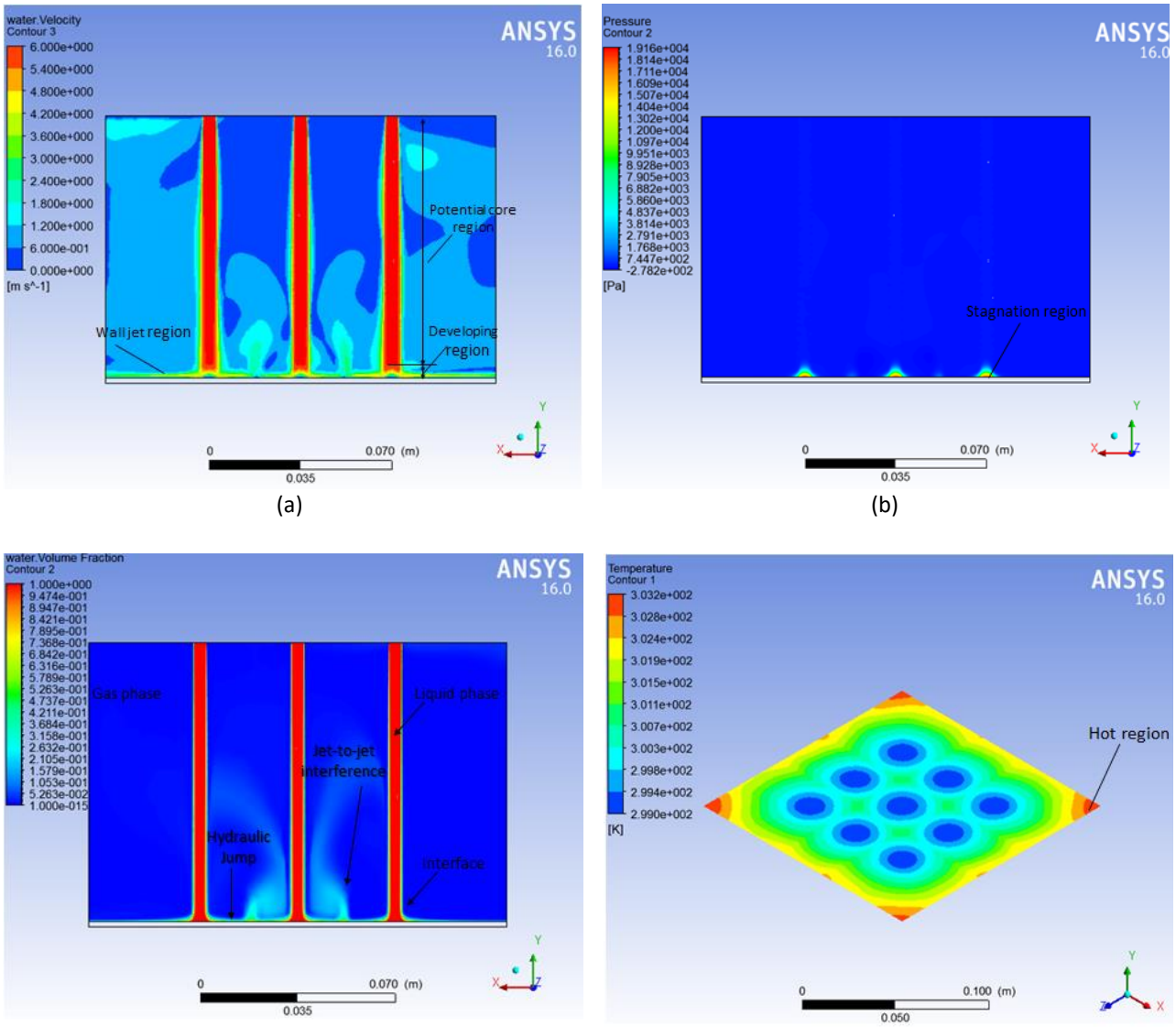


**Fig. 10.** Flow structure of the inline jet impingement at (a) the stagnation region (b) axial velocity degradation (c) interface between water and air entrainment and (d) temperature distribution on the target plate

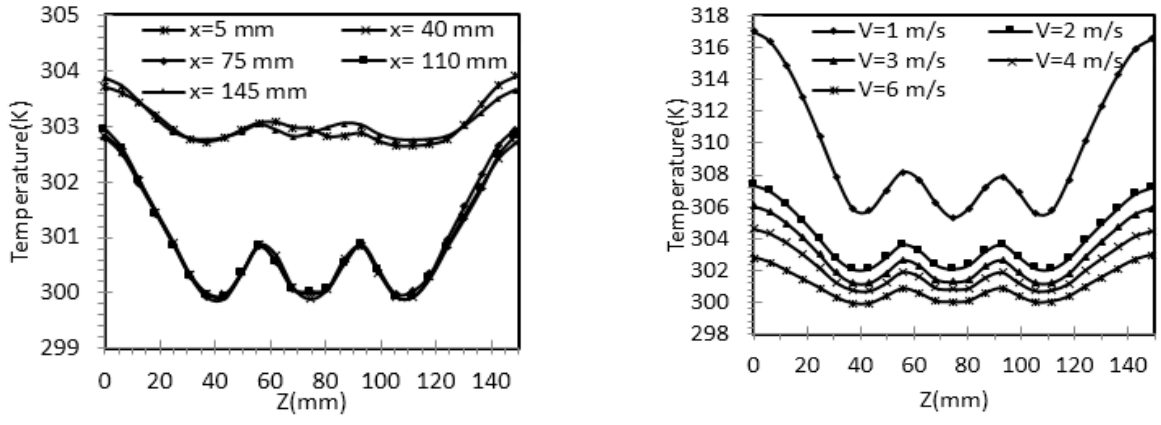


**Fig. 11.** Temperature distribution on the target plate of 9-inline jet array, (a) local temp. along Z-axis at different X values and (b) local temp. along Z-axis and at X=75 mm for different jet velocity

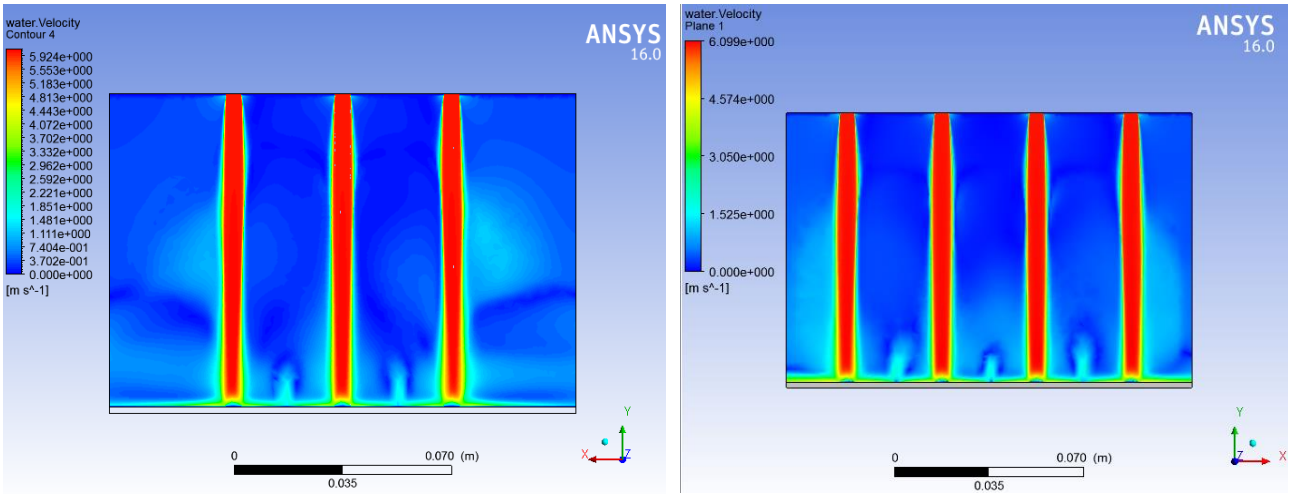


(a) (b)

**Fig. 12.** Velocity contours at $v_{jet}$=6 m/s; (a) inline and (b) staggered

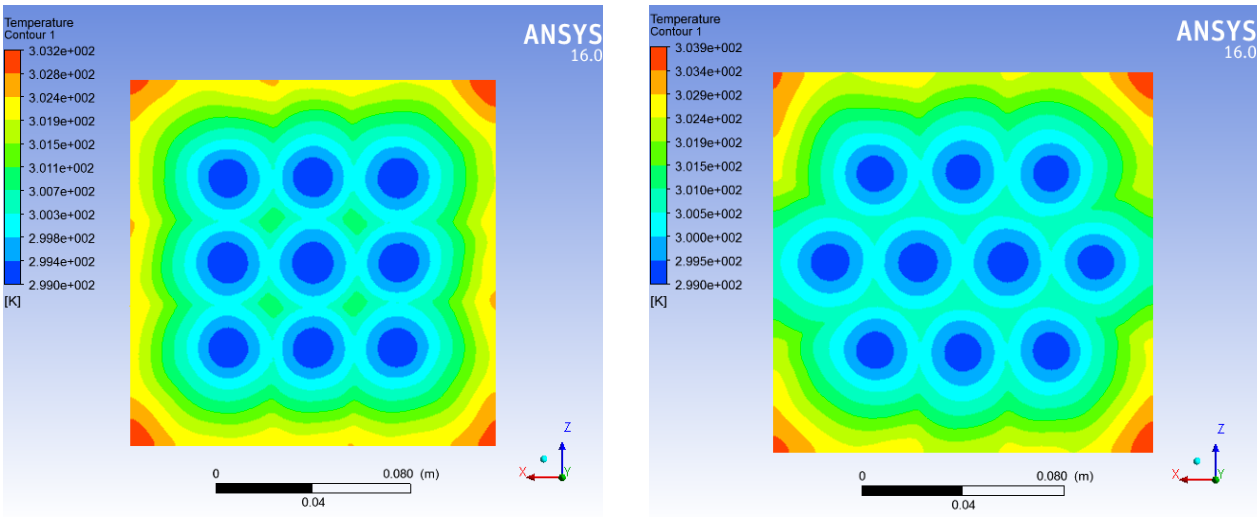


(a) (b)

**Fig. 13.** Surface temperature contours at $v_{jet}$=6 m/s; a-inline, b-staggered

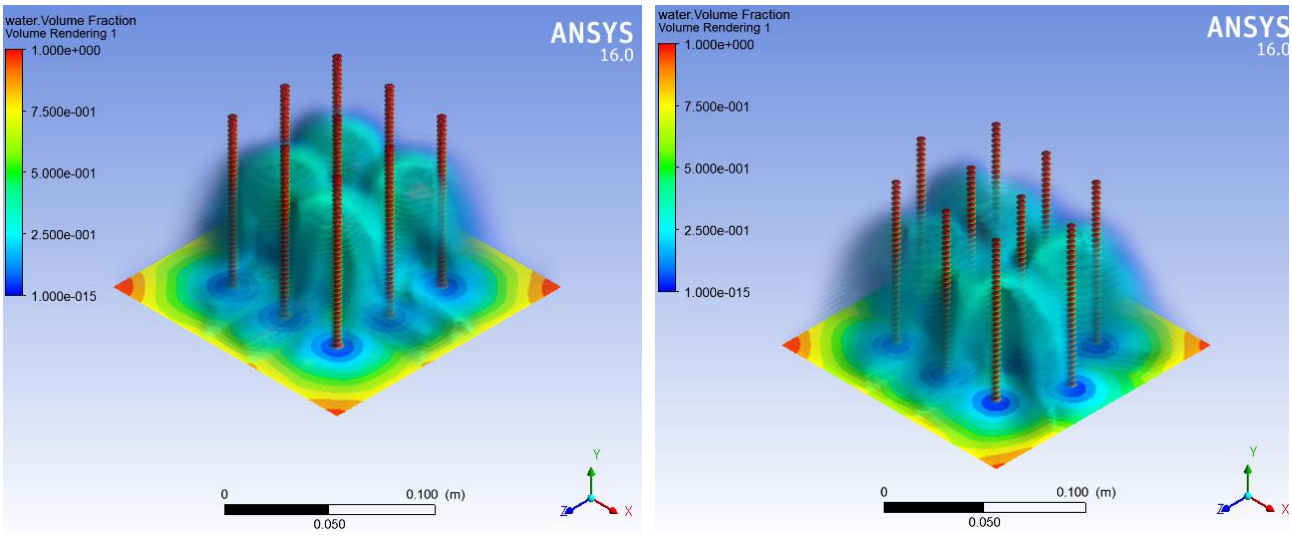


(a) (b)

**Fig. 14.** Water volume fraction rending at $V_{jet}$=6 m/s for; a- inline, b-staggered

### *4.2 Jet-to-target Spacing Optimization*

Wu *et al.,* [41] conducted their experiments on a single free surface jet impingement using $Al_2O_3$ nanofluid, they determined the best jet to target distance which is gave the best thermal effectiveness, $H/D_{jet}$ varied as 6.6, 10.5 and 19.7 they found that heat transfer coefficients increased with decreasing H, however, for very small H the thermal performance decreasing due to the back slash effect which appear at $H/D_{jet}$=6.6, the best results found at $H/D_{jet}$=10. In the present study Nozzle-to-target distance (H) for different jet plates is optimized for the maximum heat transfer performance, water is used as a working fluid, $V_{jet}$ varied from 1 to 6 m/s, $H/D_{jet}$=10, 20, 30 and 40. 9 inline jets plate is employed, the relation between jet Reynolds number with average Nusselt number on the target plate is obtained in Figure 15, the data show that, the lowest thermal performance occurred at $H/D_{jet}$=40 this happens because, the jets plate is located far away from the target plate compared to other cases, at low jet Reynolds number ,$H/D_{jet}$=10 show the best performance than others followed by $H/D_{jet}$=20 but, this result is reversed at high jet Reynolds number due to the back slash effect. The best overall thermal performance is obtained by $H/D_{jet}$=20.

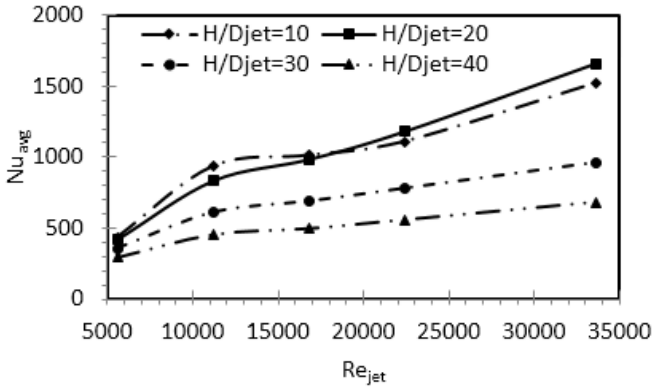


**Fig. 15.** Jet to target space determination

### *4.3 Effect of Jet Configurations*

Heat transfer behavior and fluid flow characteristics of inline and staggered free surface jet arrays hitting a hot plate are investigated. Water and $Al_2O_3$-water nanofluid were employed as working fluids, three nanofluid volume concentrations were tested; 5%, 8% and 10%. For inline array and from numerical results, average Nusselt numbers increased by 7%, 25% and 48% for 5%, 8% and 10% volume fraction respectively and 6 m/s jet velocity compared with water at the same conditions (Figure 16(a)). Average surface temperature at φ=10% and 1 m/s jet velocity is 305.3 K which is less than water by 8.4 K. Minimum local surface temperature at X=0 mm, $V_{jet}$=2 m/s is 298.8 K at the impingement point and 10% concentration which is 4 K less than water at the same conditions, maximum local surface temperature at X=0 mm $V_{jet}$=2 m/s was 307.3 K(hot region) at 0% concentration(water) and 2 m/s jet velocity at the target edges while the maximum temperature at 10% volume fraction was 304.1 K at the same flow rate (Figure 16(b)). For staggered array and from numerical results, average Nusselt numbers increased by 17%, 27% and 57% for 5%, 8% and 10% volume fraction respectively and 6 m/s jet velocity compared with water at the same conditions (Figure 17(a)). Average surface temperature at φ=10% and 1 m/s jet velocity is 304 K which is less than water by 8 K. Minimum local surface temperature at X=0 mm, $V_{jet}$=2 m/s is 298.1 K at the impingement point and 10% concentration which is 3.2 K less than water at the same conditions, maximum local surface temperature at X=0 mm $V_{jet}$=2 m/s was 304 K(hot region) at 0%

concentration(water) and 2 m/s jet velocity at the target edges while the maximum temperature at 10% volume fraction was 300.4 K at the same flow rate (Figure 17(b)). Figure 18 shows the average Nusselt number for Nanofluid volume fractions of 5% and 10% respectively, the highest heat transfer performance can be obtained by staggered jets plate followed by inline jets plate at the same jet velocity. The enhancement of heat transfer is markedly shown at higher jet velocities and nanofluid volume fraction.

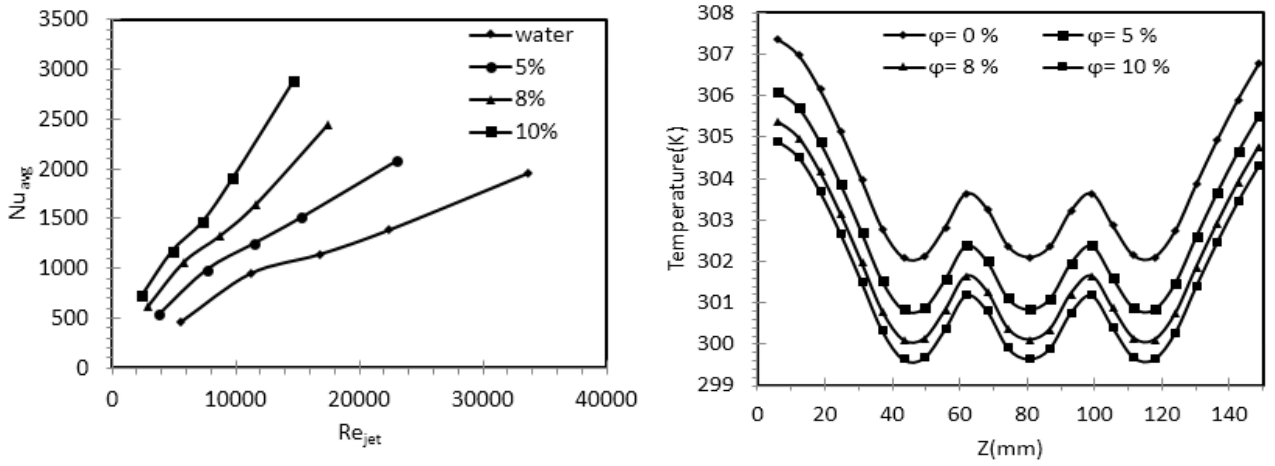


(a) (b)

**Fig. 16.** Inline array; (a) average Nusselt numbers with jet Reynolds number and (b) local temperature on target plate at X=75 mm along the Z-axis and $V_{jet}$=2 m/s

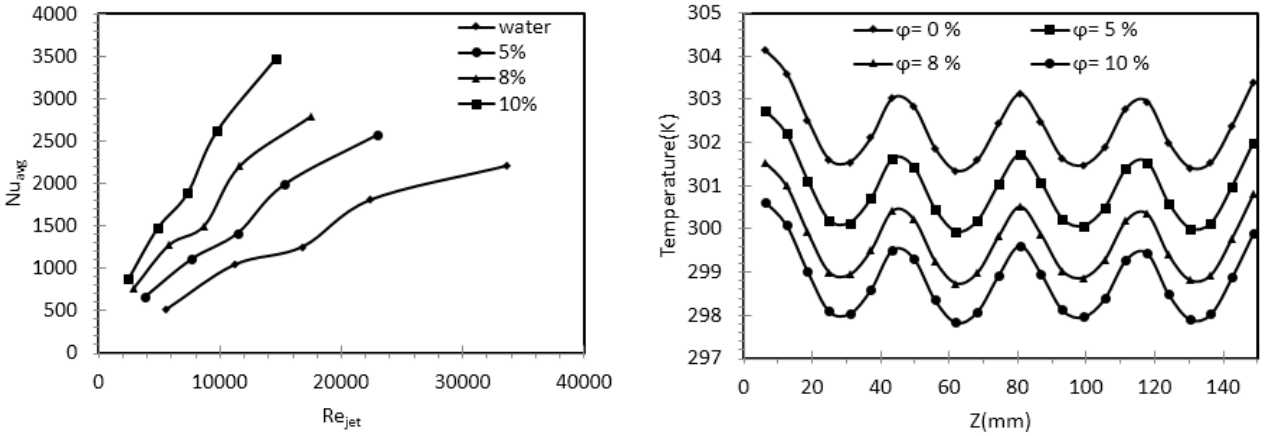


(a) (b)

**Fig. 17.** Staggered array; (a) average Nusselt numbers with jet Reynolds number, (b) local temperature on target plate at X=75 mm along the Z-axis and $V_{jet}$=2 m/s

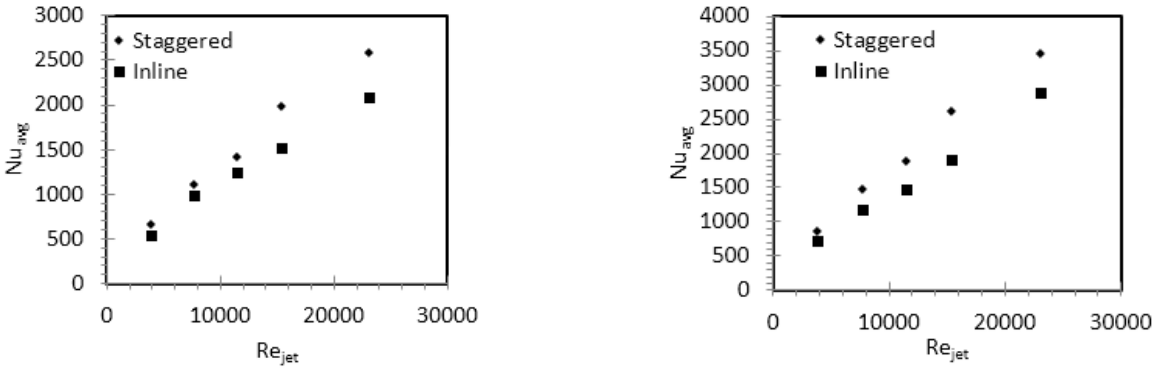

(a) (b)

**Fig. 18.** Average Nusselt numbers for nanofluid volume fractions of (a) φ=5% and (b) φ=10% inline and staggered jet arrays

### *4.4 Correlation Equations of the Experimental Work*

Nanofluid free surface jet impingement heat transfer behaviour and fluid flow characteristics are influenced by the fluid physical and thermal properties (Density, viscosity, thermal conductivity, Reynolds, Prandtl, Péclet numbers and nanofluid concentration) and the geometrical parameters ($D_{jet}$, $H/D_{jet}$ and $Xn/D_{jet}$). Generally, according to the previous studies of Liu and Lienhard [42] and Viskanta [43], the relation between jet Reynolds number and average Nusselt number can be expressed as;

$$Nu_{avg} = C\ Re^{m} Pr^{n} \tag{17}$$

Xuan and Roetzel [44] were considered nanofluid effects on the heat transfer equation and their correlation can be expressed as;

$$Nu_{avg} = A(1 + Pe^{B}\phi^{C})Re^{D} Pr^{E} \tag{18}$$

According to the study of Ma *et al.,* [45], when Pr>3, E=1/3, when 0.15<Pr<3, E=0.4. For the present experiments the Pr>6 so that; E=1/3. From experimental results and using the Rstudio commercial software, all coefficients in Eq. (18) can be calculated for different jet configurations. Table 4 shows the correlation equations for inline and staggered jets, and the study limitations are; Reynolds number range 2441≤Re ≤33611, Prandtl number 6.04≤Pr ≤9.68, $Al_2O_3$-water nanofluid concentration 0% ≤φ ≤10% range and $H/D_{jet}$ =20. Figure 19 show the relation measured and calculated values of Nusselt numbers, it can be illustrated that the maximum deviation is ±10 %.

**Table 4**
Correlation equations of free surface jet impingement cooling system

| Case | Equation | $R^2$ |
|---|---|---|
| Inline | $Nu_{avg} = 0.75\left(1 + Pe^{0.38}\phi^{1.89}\right)Re^{0.68}Pr^{\frac{1}{3}}$ (19) | 0.993 |
| Staggered | $Nu_{avg} = 0.76(1 + Pe^{0.36}\phi^{1.64})Re^{0.71}Pr^{1/3}$ (20) | 0.992 |

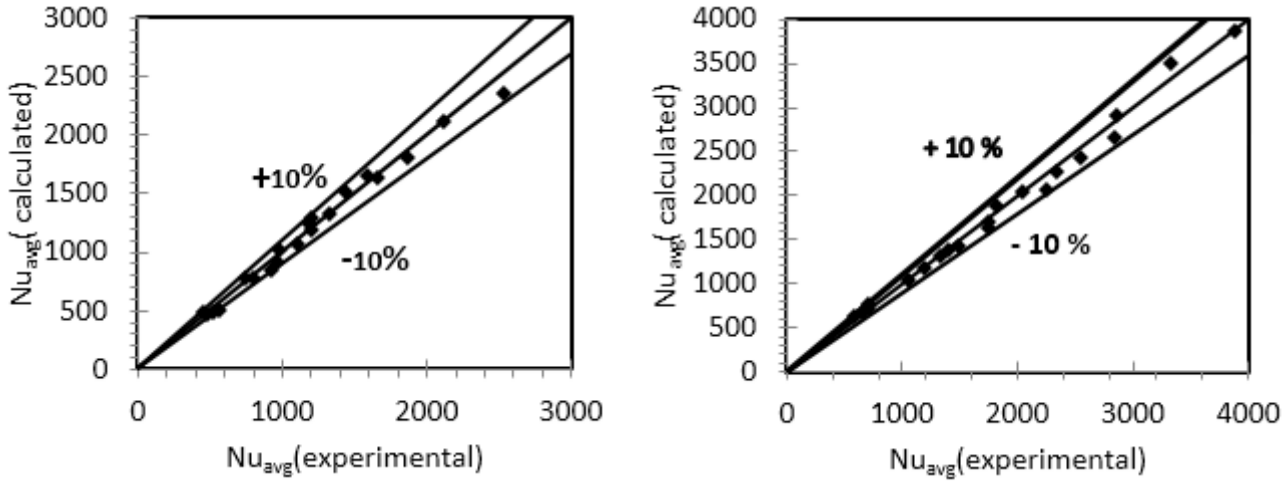

(a) (b)

**Fig. 19.** Comparison between the calculated and the experimental Nusselt numbers; (a) inline and (b) staggered

## 5. Conclusions

Heat transfer enhancement of the multiple free surface jet impingement cooling system is investigated experimentally and numerically. It can be concluded that

i. $Al_2O_3$-water nanofluid enhances heat transfer more than water at the same condition in both inline and staggered arrays. Such enhancement is markedly evident at higher jet velocities, nanofluid volume fraction and number of jets.
ii. Using $Al_2O_3$ nanofluid as a coolant instead of water can decrease average and local surface temperature distribution which influence heat transfer behavior and fluid flow characteristics on the target plate and the best performance of nanofluid obtained at high Reynolds numbers.
iii. Minimum surface temperature was occurred at the impingement zones while maximum temperature obtained at the target plate edges
iv. CFD model with k-ε turbulence model presents a good agreement of heat transfer coefficient in comparison with experimental results at low jet Reynolds number.
v. The best Nusselt number is obtained by staggered jet arrays at 6 m/s and 10% nanofluid concentration followed by inline jet array.
vi. The correlation equations for inline and staggered arrays show a good agreement with the experimental results at the same conditions.

The study limitations can be concluded as

i. For the experimental study, the measurements of pressure drop and friction factor are neglected; hence, the cooling system efficiency is not included in this investigation.
ii. There is an obvious variation between numerical and experimental results at high Reynolds numbers and this variation may be due to using a single-phase model to simulate the nanofluid, so it is recommended for a future work using two-phase model.
iii. Some important factors such as; $H/D_{jet}$ and $X_n/D_{jet}$ are not included in the correlation equation.

## Acknowledgement

This research was funded by a grant from Ministry of Higher Education, Beni-Suef University, Egypt.

## References

[1] Molana, M., and Salem Banooni. "Investigation of heat transfer processes involved liquid impingement jets: a review." *Brazilian Journal of Chemical Engineering* 30, no. 3 (2013): 413-435.
[2] Bula, Antonio J., Muhammad M. Rahman, and John E. Leland. "Axial steady free surface jet impinging over a flat disk with discrete heat sources." *International Journal of Heat and Fluid Flow* 21, no. 1 (2000): 11-21.
[3] Lienhard, John H. "Heat transfer by impingement of circular free-surface liquid jets." In *Proceedings of 18th National and 7th ISHMT-ASME Heat and Mass Transfer Conference, Guwahati, India*. 2006.
[4] Baonga, J. Bosco, H. Louahlia-Gualous, and Michel Imbert. "Experimental study of the hydrodynamic and heat transfer of free liquid jet impinging a flat circular heated disk." *Applied Thermal Engineering* 26, no. 11-12 (2006): 1125-1138.
[5] Han, B., and Richard J. Goldstein. "Jet-impingement heat transfer in gas turbine systems." *Annals of the New York Academy of Sciences* 934, no. 1 (2001): 147-161.
[6] Hollworth, B. R., and R_ D. Berry. "Heat transfer from arrays of impinging jets with large jet-to-jet spacing." (1978): 352-357.

[7] Obot, N. T., and T. A. Trabold. "Impingement heat transfer within arrays of circular jets: Part 1—Effects of minimum, intermediate, and complete crossflow for small and large spacings." *Journal of Heat transfer* 109, no. 4 (1987): 872-879.
[8] Robinson, A. J., and E. Schnitzler. "An experimental investigation of free and submerged miniature liquid jet array impingement heat transfer." *Experimental Thermal and Fluid Science* 32, no. 1 (2007): 1-13.
[9] Geers, L. F. G., M. J. Tummers, T. J. Bueninck, and K. Hanjalić. "Heat transfer correlation for hexagonal and in-line arrays of impinging jets." *International Journal of Heat and Mass Transfer* 51, no. 21-22 (2008): 5389-5399.
[10] Womac, D. J., S. Ramadhyani, and F. P. Incropera. "Correlating equations for impingement cooling of small heat sources with single circular liquid jets." (1993): 106-115.
[11] Brakmann, Robin, Lingling Chen, Bernhard Weigand, and Michael Crawford. "Experimental and numerical heat transfer investigation of an impinging jet array on a target plate roughened by cubic micro pin fins." *Journal of Turbomachinery* 138, no. 11 (2016): 111010.
[12] Wan, Chaoyi, Yu Rao, and Xiang Zhang. "Numerical investigation of impingement heat transfer on a flat and square pin-fin roughened plates." In *ASME Turbo Expo 2013: Turbine Technical Conference and Exposition*. American Society of Mechanical Engineers Digital Collection, 2013.
[13] Weigand, Bernhard, and Sebastian Spring. "Multiple jet impingement– a review." *Heat Transfer Research* 42, no. 2 (2011).
[14] Masoumi, N., N. Sohrabi, and A. Behzadmehr. "A new model for calculating the effective viscosity of nanofluids." *Journal of Physics D: Applied Physics* 42, no. 5 (2009): 055501.
[15] Xiangqi, Wang. "New approaches to micro-electronic component cooling." PhD diss., 2007.
[16] Palm, Samy Joseph, Gilles Roy, and Cong Tam Nguyen. "Heat transfer enhancement with the use of nanofluids in radial flow cooling systems considering temperature-dependent properties." *Applied Thermal Engineering* 26, no. 17-18 (2006): 2209-2218.
[17] Yang, Yue-Tzu, and Feng-Hsiang Lai. "Numerical study of heat transfer enhancement with the use of nanofluids in radial flow cooling system." *International Journal of Heat and Mass Transfer* 53, no. 25-26 (2010): 5895-5904.
[18] Feng, Yu, and Clement Kleinstreuer. "Nanofluid convective heat transfer in a parallel-disk system." *International Journal of Heat and Mass Transfer* 53, no. 21-22 (2010): 4619-4628.
[19] Kumar, R., and Nigussie Mulugeta. "Inline array jet impingement cooling using Al2O3/water nanofluid in a plate finned electronic heat sink." *AJER* 3, no. 3 (2014): 188-196.
[20] Manca, Oronzio, Paolo Mesolella, Sergio Nardini, and Daniele Ricci. "Numerical study of a confined slot impinging jet with nanofluids." *Nanoscale Research Letters* 6, no. 1 (2011): 188.
[21] Maghrebi, Mohammad Javad, Taher Armaghani, and Farhad Talebi. "Effects of nanoparticle volume fraction in hydrodynamic and thermal characteristics of forced plane jet." *Thermal Science* 16, no. 2 (2012): 455-468.
[22] Huang, Jun-Bo, and Jiin-Yuh Jang. "Numerical study of a confined axisymmetric jet impingement heat transfer with nanofluids." *Engineering* 5, no. 1 (2013): 69.
[23] Siddiqui, Md Irfanul Haque, and Pradeep Kumar Jha. "Assessment of turbulence models for prediction of intermixed amount with free surface variation using coupled level-set volume of fluid method." *ISIJ International* 54, no. 11 (2014): 2578-2587.
[24] Yang, Yue-Tzu, Yi-Hsien Wang, and Jen-Chi Hsu. "Numerical thermal analysis and optimization of a water jet impingement cooling with VOF two-phase approach." *International Communications in Heat and Mass Transfer* 68 (2015): 162-171.
[25] Davarnejad, Reza, and Maryam Jamshidzadeh. "CFD modeling of heat transfer performance of MgO-water nanofluid under turbulent flow." *Engineering Science and Technology, an International Journal* 18, no. 4 (2015): 536-542.
[26] Isman, M. K., E. Pulat, A. B. Etemoglu, and M. Can. "Numerical investigation of turbulent impinging jet cooling of a constant heat flux surface." *Numerical Heat Transfer, Part A: Applications* 53, no. 10 (2008): 1109-1132.
[27] Roy, Gilles, Cong Tam Nguyen, and Paul-René Lajoie. "Numerical investigation of laminar flow and heat transfer in a radial flow cooling system with the use of nanofluids." *Superlattices and Microstructures* 35, no. 3-6 (2004): 497-511.
[28] Hasan, Husam Abdulrasool, Kamaruzzaman Sopian, Ahed Hameed Jaaz, and Ali Najah Al-Shamani. "Experimental investigation of jet array nanofluids impingement in photovoltaic/thermal collector." *Solar Energy* 144 (2017): 321-334.
[29] Ghadimi, A., Rahman Saidur, and H. S. C. Metselaar. "A review of nanofluid stability properties and characterization in stationary conditions." *International Journal of Heat and Mass Transfer* 54, no. 17-18 (2011): 4051-4068.
[30] Wang, Xian-ju, and Dong-sheng Zhu. "Investigation of pH and SDBS on enhancement of thermal conductivity in nanofluids." *Chemical Physics Letters* 470, no. 1-3 (2009): 107-111.
[31] Maxwell, J. C. "A treatise on electricity and magnetism., Vol. 1 Clarendon Press." (1873).

[32] Fick, Rutger, Demian Wassermann, and Rachid Deriche. "Mipy: an open-source framework to improve reproducibility in brain microstructure imaging." 2018.
[33] Xuan, Yimin, Qiang Li, and Weifeng Hu. "Aggregation structure and thermal conductivity of nanofluids." *AIChE Journal* 49, no. 4 (2003): 1038-1043.
[34] Handbook, A. S. H. R. A. E. "Fundamentals, american society of heating refrigeration and air-conditioning engineers." *Inc. Atlanta, GA* (2005).
[35] Li, Ping, Di Zhang, and Yonghui Xie. "Heat transfer and flow analysis of Al2O3–water nanofluids in microchannel with dimple and protrusion." *International Journal of Heat and Mass Transfer* 73 (2014): 456-467.
[36] Kline, Stephen J. "Describing uncertainty in single sample experiments." *Mech. Engineering* 75 (1953): 3-8.
[37] Zhang, Yuwen, and Amir Faghri. "Analysis of forced convection heat transfer in microencapsulated phase change material suspensions." *Journal of Thermophysics and Heat Transfer* 9, no. 4 (1995): 727-732.
[38] Sahoo, Bhaskar C., Ravikanth S. Vajjha, Rajive Ganguli, Godwin A. Chukwu, and Debendra K. Das. "Determination of rheological behavior of aluminum oxide nanofluid and development of new viscosity correlations." *Petroleum Science and Technology* 27, no. 15 (2009): 1757-1770.
[39] Tang, Clement C., Sanjib Tiwari, and Matthew W. Cox. "Viscosity and friction factor of aluminum oxide–water nanofluid flow in circular tubes." *Journal of Nanotechnology in Engineering and Medicine* 4, no. 2 (2013): 021004.
[40] CFX-Solver, A. N. S. Y. S. "Theory guide." *Release ll* (2006).
[41] Wu, W., H. Bostanci, L. C. Chow, S. J. Ding, Y. Hong, M. Su, John P. Kizito, L. Gschwender, and C. E. Snyder. "Jet impingement and spray cooling using slurry of nanoencapsulated phase change materials." *International Journal of Heat and Mass Transfer* 54, no. 13-14 (2011): 2715-2723.
[42] Liu, X., and J. H. Lienhard. "Extremely high heat fluxes beneath impinging liquid jets." *ASME Transactions Journal of Heat Transfer* 115 (1993): 472-476.
[43] Viskanta, R. "Heat transfer to impinging isothermal gas and flame jets." *Experimental Thermal and Fluid Science* 6, no. 2 (1993): 111-134.
[44] Xuan, Yimin, and Wilfried Roetzel. "Conceptions for heat transfer correlation of nanofluids." *International Journal of Heat and Mass Transfer* 43, no. 19 (2000): 3701-3707.
[45] Ma, C. F., Y. P. Gan, Y. C. Tian, D. H. Lei, and T. Gomi. "Liquid jet impingement heat transfer with or without boiling." *Journal of Thermal Science* 2, no. 1 (1993): 32.